PAPER

Structure of bismuth tellurite and bismuth niobium tellurite glasses and $Bi_2Te_4O_{11}$ anti-glass by high energy X-ray diffraction

Nupur Gupta, [ID][a] Atul Khanna, [ID] *[a] Hirdesh,[a] Ann-Christin Dippel [ID][b] and Olof Gutowski[b]

Glass and anti-glass samples of bismuth tellurite ($x Bi_2O_3$–(100 − x)TeO_2) and bismuth niobium tellurite ($x Bi_2O_3$–$x Nb_2O_5$–(100 − 2x)TeO_2) systems were prepared by melt-quenching. The bismuth tellurite system forms glasses at low Bi_2O_3 concentration of 3 to 7 mol%. At 20 mol% Bi_2O_3, the glass forming ability of the Bi_2O_3–TeO_2 system decreases drastically and the anti-glass phase of monoclinic $Bi_2Te_4O_{11}$ is produced. Structures of glass and the anti-glass $Bi_2Te_4O_{11}$ samples were studied by high-energy X-ray diffraction, reverse Monte Carlo simulations and Rietveld Fullprof refinement. All glasses have short short-range disorder due to the existence of at least three types of Te–O bonds of lengths: 1.90, 2.25 and 2.59 Å, besides a variety of Bi–O and Nb–O bond-lengths. The medium-range order in glasses is also disturbed due to the distribution of Te–Te pair distances. The average Te–O co-ordination (N_{Te-O}) in the glass network decreases with an increase in Bi_2O_3 and Nb_2O_5 mol% and is in the range: 4.17 to 3.56. The anti-glass $Bi_2Te_4O_{11}$ has a long-range order of cations but it has vibrational disorder and it exhibits sharp X-ray reflections but broad vibrational bands similar to that in glasses. Anti-glass $Bi_2Te_4O_{11}$ has an N_{Te-O} of 2.96 and is significantly lower than in glass samples.

1. Introduction

Tellurite glasses are of great significance in the field of optics owing to their distinctive properties which marks them as outstanding materials for applications in third order harmonic generation, optical waveguides, and Raman amplifiers.[1–5] TeO_2 forms glass only at a high melt cooling rate ($\sim 10^5$ K s^{-1}) by roller quenching[6] or by intermittent cooling techniques,[7] however, its glass forming ability (GFA) enhances considerably upon the addition of modifier oxides such as alkali, alkaline-earth and heavy metal oxides.[6–9] The basic structural units of the tellurite glasses are trigonal bipyramidal (TeO_4) and trigonal pyramidal (TeO_3) units. When a modifier oxide is added into the TeO_2 glass, it breaks the Te–O–Te linkages and forms trigonal (TeO_3) units.

The incorporation of Bi_2O_3 into the Te–O network enhances the non-linear optical properties of the tellurite glasses.[10–13] However, bismuth tellurite system forms glass only at a low concentration of Bi_2O_3 (up to 7 mol%), while at higher concentration of 20 mol% Bi_2O_3, it forms a purely anti-glass monoclinic $Bi_2Te_4O_{11}$ on melt quenching.[14] An anti-glass is an intermediate, transient phase which has features of both the glassy and crystalline solids, in which the cations (Bi^{3+}, Te^{4+},

Nb^{5+} *etc.*) possess long-range order but the anions (oxygens) are highly disordered and the anion sites are partially vacant.[15–17] The cationic order is responsible for producing sharp peak reflections in the X-ray and neutron diffraction patterns, while the anionic defects do not allow the phonons to propagate through them for long distances, thus resulting in the broad vibrational (phonon) bands in the Raman and infrared spectra.[18,19]

Bismuth tellurite glasses have been studied for their optical and structural properties[13,20] but the information about the short-range and medium-range order of bismuth tellurite glass system is not available. The addition of Nb_2O_5 in $x Bi_2O_3$–(100 − x)TeO_2 system enhances its GFA and produces glass–ceramic samples that contain coexisting glass and anti-glass phases on slow melt-cooling. The database of glass short-range structural properties such as cation–oxygen bond lengths, co-ordination numbers and bond angle distributions is required for the fundamental understanding of glassy materials, making structure–property correlations, for the mathematical modeling of glass density, elastic moduli, linear and non-linear refractive indices, stress–optical properties and for machine learning.[21–24]

Wilding *et al.*[25] studied the structure of binary and ternary tellurite glasses within the system: Bi_2O_3–Nb_2O_5–TeO_2 by high energy X-ray diffraction. These studies revealed a glassy network consisting of interconnected TeO_4 and TeO_3 units correlated to the crystalline TeO_2 materials but possessing larger Te···Te separations due to the presence of TeO_3 groups and non-

[a]*Department of Physics, Guru Nanak Dev University, Amritsar-143005, Punjab, India. E-mail: atul.phy@gndu.ac.in; Fax: +91-183-2258820; Tel: +91-183-2258802 ext. 3568*
[b]*Deutsches Elektronen-Synchrotron DESY, Notkestrasse 85, 22607 Hamburg, Germany*

Table 1 Composition, density and atomic number density of bismuth tellurite and bismuth niobium tellurite samples

Sample code	Composition (mol%)			Density (g cm^{-3}) ($\pm$0.001)	Number density (Å^{-3})
	Bi$_2$O$_3$	Nb$_2$O$_5$	TeO$_2$		
3BiTe	3	—	97	6.001	0.0655
5BiTe	5	—	95	6.122	0.0653
7BiTe	7	—	93	6.191	0.0646
20BiTe	20	—	80	6.894	0.0639
5Bi5NbTe	5	5	90	5.807	0.0640
7.5Bi7.5NbTe	7.5	7.5	85	5.921	0.0645
10Bi10NbTe	10	10	80	5.995	0.0646
12.5Bi12.5NbTe	12.5	12.5	75	6.083	0.0650

Table 2 X-ray scattering weight factors, W_{ij} (%) for the atomic pairs in bismuth tellurite glasses at $Q = 5.01$ Å^{-1}

Atomic pair	3BiTe	5BiTe	7BiTe
Bi–Bi	0.584	1.51	2.76
Bi–Te	11.75	17.87	22.83
Bi–O	2.351	3.69	4.86
Te–Te	59.22	52.85	47.26
Te–O	23.72	21.82	20.13
O–O	2.37	2.52	2.14

Table 3 X-ray scattering weight factors, W_{ij} (%) for the atomic pairs in bismuth niobium tellurite glasses at $Q = 5.01$ Å^{-1}

Atomic pair	5Bi5NbTe	7.5Bi7.5NbTe	10Bi10NbTe	12.5Bi12.5NbTe
Bi–Bi	1.42	2.86	4.56	6.45
Bi–Nb	1.35	2.72	4.35	6.14
Bi–Te	15.90	20.14	22.72	24.05
Bi–O	3.71	5.21	6.51	7.67
Nb–Nb	0.32	0.64	1.04	1.46
Nb–Te	7.58	9.60	10.83	11.47
Nb–O	1.77	2.48	3.11	3.66
Te–Te	44.61	35.53	28.29	22.47
Te–O	20.87	18.40	16.24	14.34
O–O	2.44	2.38	2.33	2.29

Table 4 Atomic number density and half-box length values used in RMC simulations on bismuth tellurite and bismuth niobium tellurite glasses

Sample code	Number density (Å^{-3})	Half-box length Å
3BiTe	0.0655	26.72
5BiTe	0.0653	26.74
7BiTe	0.0646	26.83
5Bi5NbTe	0.0640	26.92
7.5Bi7.5NbTe	0.0645	26.85
10Bi10NbTe	0.0646	26.83
12.5Bi12.5NbTe	0.0650	26.78

Table 5 Cut-off distances used for atomic pairs used in the final RMC simulation for bismuth tellurite glasses

Atomic pair	Sample code		
	3BiTe (Å)	5BiTe (Å)	7BiTe (Å)
Bi–Bi	3.65	3.65	3.65
Bi–Te	3.00	3.00	3.00
Bi–O	1.82	1.84	1.84
Te–Te	2.80	2.88	2.95
Te–O	1.67	1.67	1.67
O–O	2.32	2.32	2.32

bridging oxygens (NBOs) that are linked to modifier (Bi^{3+}, and Nb^{5+}) cations. It was found that the mean Te–O coordination number for TeO$_2$-rich compositions to be ~3.7 (98% Bi$_2$O$_3$) and ~3.8 (98% Nb$_2$O$_5$) signifying the presence of TeO$_3$ and TeO$_4$ polyhedra (dominated by TeO$_4$) that are both corner- and edge-shared.

In the present work, the high energy X-ray diffraction (HEXRD) studies were carried out on glass, and anti-glass samples of xBi$_2$O$_3$–(100 − x)TeO$_2$ and xBi$_2$O$_3$–xNb$_2$O$_5$–(100 − 2x)TeO$_2$ systems. The diffraction data of glasses was analyzed by Reverse Monte Carlo (RMC) simulations, the latter is a powerful tool to

Table 6 Cut-off distances used for each atomic pair in the final RMC simulation for bismuth niobium tellurite glasses

Atomic pair	Sample code			
	5Bi5NbTe (Å)	7.5Bi7.5NbTe (Å)	10Bi10NbTe (Å)	12.5Bi12.5NbTe (Å)
Bi–Bi	3.45	3.45	3.45	3.45
Bi–Nb	3.30	3.30	3.30	3.30
Bi–Te	3.00	3.00	3.00	3.00
Bi–O	1.82	1.79	1.82	1.82
Nb–Nb	3.60	3.60	3.40	3.40
Nb–Te	3.00	3.20	2.90	2.90
Nb–O	1.69	1.69	1.72	1.72
Te–Te	2.80	2.75	2.80	2.75
Te–O	1.67	1.67	1.69	1.69
O–O	2.32	2.32	2.32	2.32

study the short-range structural properties such as bond-lengths, bond-angles and the average coordination numbers in disordered materials.[26] The use of high energy X-rays and large area detectors provides access to high values of momentum transfer function, Q with the additional advantage of smaller polarization corrections due to smaller diffraction angles (maximum used 2θ $\sim40°$).[27]

The diffraction data of the anti-glass sample: $20Bi_2O_3$–$80TeO_2$ ($Bi_2Te_4O_{11}$) was analyzed by Rietveld refinement in order to obtain the detailed crystal structure information including the Te and Bi co-ordination numbers, the cation–oxygen bond lengths and the unit cell parameters.[28] Short-range structures of glass and anti-glass phases of the bismuth tellurite system were also characterized by Raman spectroscopy.

2. Experimental details

2.1. Sample preparation

The samples of the following compositions were prepared:

(i) xBi_2O_3–$(100 - x)TeO_2$; $x = 3, 5, 7$ and 20 mol%.

(ii) xBi_2O_3–xNb_2O_5–$(100 - 2x)TeO_2$; $x = 5, 7.5, 10$ and 12.5 mol%.

The appropriate amounts of raw materials of analytical reagent grade chemicals (Sigma Aldrich, India with purity of 99.9%) were weighed. The batch mixture was melted in a platinum crucible at a temperature of ~850 °C. The binary bismuth tellurite samples were fabricated by the ice quenching method where the bottom of the Pt crucible containing the melt was dipped into the ice water bath immediately after taking it out of the furnace and small flakes of the glass samples were obtained. The binary bismuth tellurite system forms glass only at low
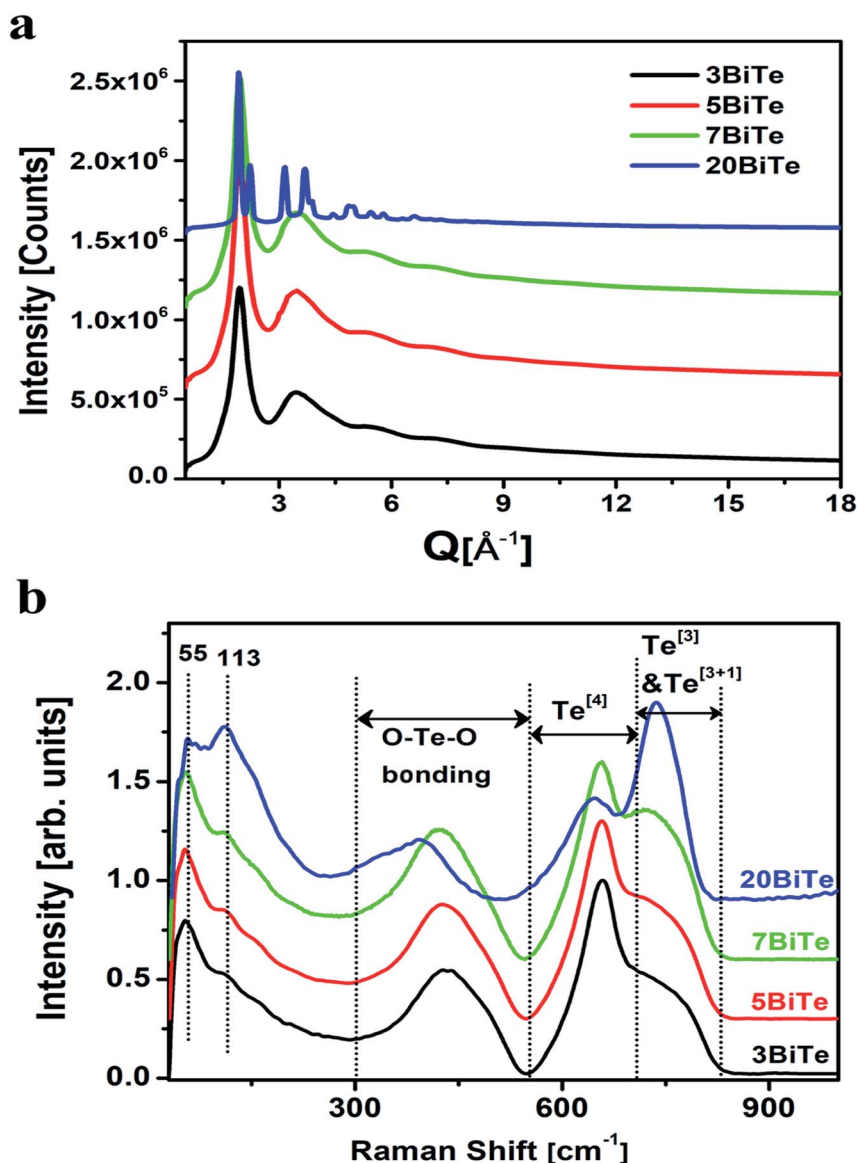

Fig. 1 (a) High-energy X-ray diffraction patterns of bismuth tellurite samples. The curves are shifted (by 1×10^6 units) for clarity (b) Raman spectra of bismuth tellurite glass and anti-glass samples.
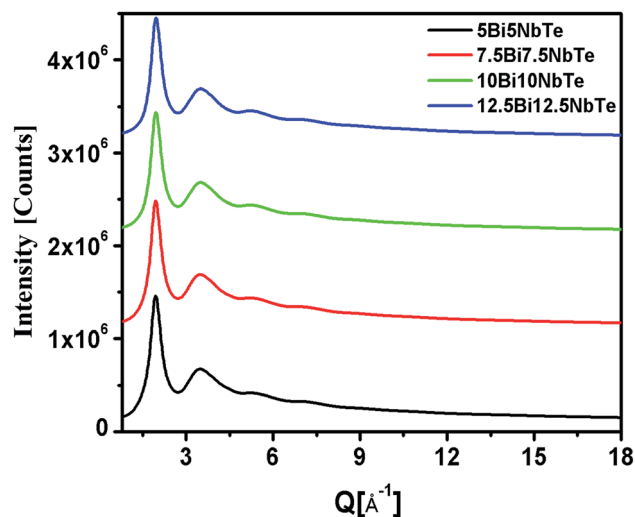
Fig. 2 High-energy X-ray diffraction patterns for bismuth niobium tellurite glasses. The curves are shifted by 1×10^6 units for clarity.

Bi_2O_3 concentration (up to 7 mol%) however, the sample with 20 mol% Bi_2O_3 formed a sample consisting entirely of mono-clinic $Bi_2Te_4O_{11}$ anti-glass phase on splat-quenching of the melt.

The melt from the ternary xBi_2O_3–xNb_2O_5–$(100 - 2x)$ TeO_2 system is reported to form co-existing glass and anti-glass phases by slow melt quench technique.[18] Hence for HEXRD studies on glasses, the glass melt from this system was splat quenched between the two metal plates to obtain thin flakes of the samples, so that the formation of anti-glass phase was avoided and purely glassy phase samples were obtained. All the samples were clear, transparent and their amorphous nature was confirmed by the laboratory source X-ray diffraction measurements performed on Bruker D8 Focus X-ray diffractometer using Cu $K_{\alpha1,2}$ radiation.

Raman spectroscopy studies were performed on Renishaw inVia Reflex micro-Raman spectrometer using 514.5 nm argon ion laser.

2.2. Density measurements

The density, ρ of the bismuth tellurite glass samples could not be measured experimentally due to their very small sizes and it was therefore calculated with the following empirical relationships given by Inaba et. al. for oxide glasses:[24]

$$\rho = \frac{\sum(M_i x_i)}{\sum(V_i x_i)} \quad (1)$$

where, M_i is the molecular weight (g mol^{-1}), x_i is the molar fraction and V_i is the packing density parameter (cm^3 mol^{-1}) for the oxide R_xO_y calculated as:

$$V_i = \frac{4}{3}\pi N_A \left(X r_M^3 + Y r_O^3\right) \quad (2)$$

N_A is the Avogadro number, r_M and r_O are the ionic radii of cations and the oxygens in the oxide, A_XO_Y.

Density of bismuth niobium tellurite samples were measured experimentally by Archimedes' principle using di-butyl phthalate as the immersion fluid.[29] The density measurements were performed three times on each sample and the maximum uncertainty in its value was ±0.002 g cm^{-3}. The sample codes, their composition, density and the atomic number density values for all the samples have are given in Table 1.

2.3. High energy X-ray diffraction

The high-energy X-ray diffraction studies were performed on bismuth tellurite glasses, bismuth niobium tellurite glasses and one bismuth tellurite anti-glass sample at High Energy Material Science beamline (P07) at PETRA III DESY photon science facility in Hamburg, Germany[30] using the wavelength of 0.126321 Å.

A double crystal monochromator consisting of two Si (111) Laue crystals was used to monochromatize the radiations obtained from the X-ray source (undulator). The scattered X-ray intensities were measured by a 2D PerkinElmer detector (model XRD1621) where the sample to detector distance was 388.2 mm. The raw intensity data were corrected for background, Compton scattering and polarization using PDFGetX2 package[31] and the structure factor, $S(Q)$ was obtained up to the 'Q' value of $\sim$20 Å^{-1}, where 'Q' refers to the momentum transfer given by $Q = 4\pi \sin\theta/\lambda$, '$\theta$' being one half of the diffraction angle and 'λ' is the wavelength of X-rays. $S(Q)$ is defined below as:[32,33]

$$S(Q) = \frac{I_x(Q) - FF(Q)}{WF(Q)} \quad (3)$$

where, $I_x(Q)$ is the measured X-ray intensity after all the corrections have been applied. $FF(Q)$ is given as $\sum_\alpha c_\alpha f_\alpha(Q) f_\alpha^*(Q)$ and $WF(Q)$ is given as $\left[\sum_\alpha c_\alpha f_\alpha(Q)\right]\left[\sum_\alpha c_\alpha f_\alpha^*(Q)\right]$ with c_α representing the concentration of element, α, and f_α is the atomic form factor of the element, α.[34] The X-ray scattering form factors depend upon Q, and the weight factors of different atomic pairs values (W_{ij}) were calculated using the formula:

$$W_{ij}(Q) = \frac{c_i f_i(Q) c_j f_j(Q)}{\left[\sum_i^k c_i f_i(Q)\right]^2} \quad (4)$$

where $f_i(Q)$ and $f_j(Q)$ are the X-ray scattering form factors of ith and j^{th} atoms in the sample, and k is the total number of elements in the system. The number of atomic pair correlations present in a glass system can be calculated using the formula: $k(k + 1)/2$. For instance, bismuth tellurite samples comprises 3 elements, namely Bi, Te and O, therefore 6 atomic pair correlations are present in it. The weight factors for different atomic pairs in bismuth tellurite and bismuth niobium tellurite glasses at $Q = 5.01$ Å^{-1} are given in Tables 2 and 3 respectively.

In this whole process, the background data was subtracted from the raw data and other corrections were applied to obtain the coherent scattering intensity (I_c), since, the latter contains

the information about the atomic structure of the sample. The Fourier-transformation was applied to the $S(Q)$ data to obtain the reduced pair distribution function, $G(r)$, given by:[35]

$$G(r) = \frac{2}{\pi} \int_{Q_{min}}^{Q_{max}} Q[S(Q) - 1]M(Q)\sin(Qr)dQ \qquad (5)$$

Q_{min} and Q_{max} represent the upper and the lower limits of the momentum transfer, Q respectively and $M(Q)$ is the Lorch modification function.

2.4. Reverse Monte Carlo (RMC) simulations

RMC simulation is a useful technique to produce the structural models of disordered materials such as glasses using the diffraction data. In the present work, the experimentally measured X-ray structure factors ($S(Q)$) for bismuth tellurite and

niobium bismuth tellurite glasses were simulated using the RMC++ software and partial atomic pair correlation functions, co-ordination numbers, and distribution of bond-lengths and bond angles were determined.[26,36–39] RMC uses a three-dimensional atomic configuration to fit the experimental $S(Q)$ data with the calculated $S(Q)$ and tends to minimize the squared difference between the two $S(Q)$ by the random movement of the atoms in the simulation box.[32,40]

As a starting model for each RMC simulation, a random atomic configuration with a simulation box containing a total of 10 000 atoms of Bi, Te, and O for bismuth tellurite system, and 10 000 atoms of Bi, Nb, Te, and O for niobium bismuth tellurite glass system was built using the density data given in Table 1. The half-box length values calculated using the number density values in the RMC++ program for all the samples are also given in Table 4.
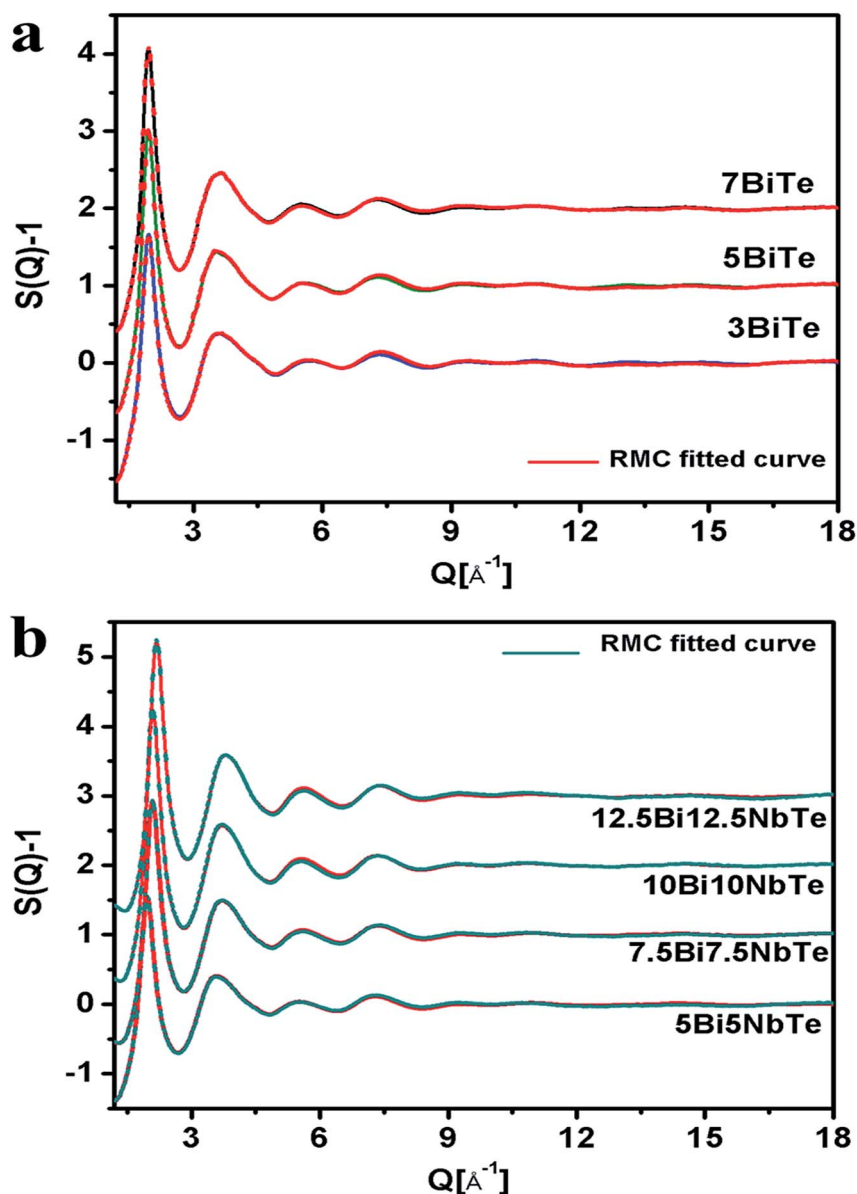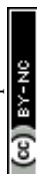

Fig. 3 Experimental and RMC fitted X-ray structure factors for (a) bismuth tellurite (b) bismuth niobium tellurite glasses (successive curves have been shifted by 1 unit for clarity).
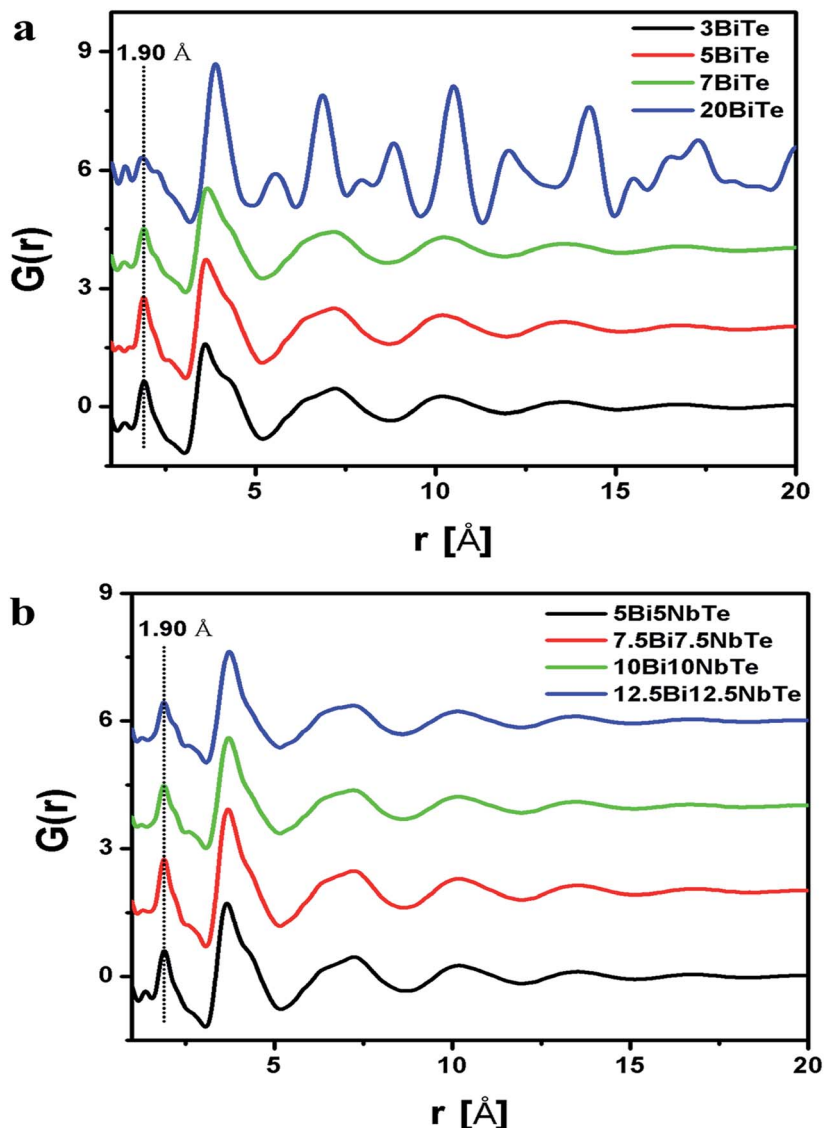
Fig. 4 Reduced pair correlation function, $G(r)$ for (a) bismuth tellurite (b) bismuth niobium tellurite samples.

As a part of the simulation, the inter-atomic distances for each atomic pair correlation was used as a constraint to fit the model with the experimental X-ray structure factor, $S(Q)$. For the three-component bismuth tellurite system, the six atomic pair correlations are Bi–Bi, Bi–Te, Bi–O, Te–Te, Te–O, and O–O, while the bismuth niobium tellurite samples contains a total of ten atomic pair correlation functions ($g_{ij}(r)$) that includes the above mentioned six and additional four correlations *i.e.* Bi–Nb, Nb–Nb, Nb–Te, and Nb–O.

The built configuration was modified by randomly moving the atoms and varying the interatomic distances slightly, until the calculated and the experimental $S(Q)$ coincided with each other perfectly and a consistent result for each partial pair correlation function $g_{ij}(r)$ and Te–O coordination number (N_{Te-O}) was obtained. The simulation results were stable and reproducible, and the broad bands in the diffraction patterns represent the short and medium-range structural features in the glasses. The cut-off distances of various correlations used in the final RMC runs for bismuth tellurite and bismuth niobium tellurite glasses are given in Tables 5 and 6

2.5. Rietveld refinement

Rietveld data analysis was performed on the HEXRD data of $Bi_2Te_4O_{11}$ anti-glass by using the Fullprof program package using the pseudo-Voigt function to model the peak profile shape. The background contribution was determined using a linear interpolation between selected data points. The initial approximation for the lattice parameters as well as structural coordinates for defining the peak shape in the powder diffraction experiment were taken from the literature.[41] The scale factor, profile shape parameters, lattice parameters, fractional coordinates of atoms, site occupations, and their displacement parameters were varied during the fitting. Once a perfect fit is obtained, and the least square value (χ^2) is minimized, the

values of bond lengths, bond angles, and the coordination number of cations with oxygen were calculated using Visualization for Electronic Structural Analysis (VESTA) software.[42]

3.   Results and discussion

3.1.   Density

The density of bismuth tellurite glasses increases from 6.001 to 6.894 g cm^{-3} with increase in Bi_2O_3 concentration from 3 to 7 mol%. The increase in the density can be attributed to the higher molecular weight of Bi_2O_3 molecules (465.96 u) as compared to the molecular weight of TeO_2 (159.60 u) which is being replaced. The incorporation of Nb_2O_5 (265.81 u) also enhances the glass density from 5.807 to 6.083 g cm^{-3} (sample code 5Bi5NbTe) due to significantly higher molecular weight of Bi_2O_3 and Nb_2O_5, both of which replace the lighter TeO_2 molecules.

3.2.   RMC analysis of HEXRD data

The XRD patterns of all the bismuth tellurite and bismuth niobium tellurite glass samples show broad humps due to their amorphous nature. However, the XRD pattern of one bismuth tellurite sample containing 20 mol% Bi_2O_3 (sample code: 20BiTe) shows sharp reflections corresponding to the
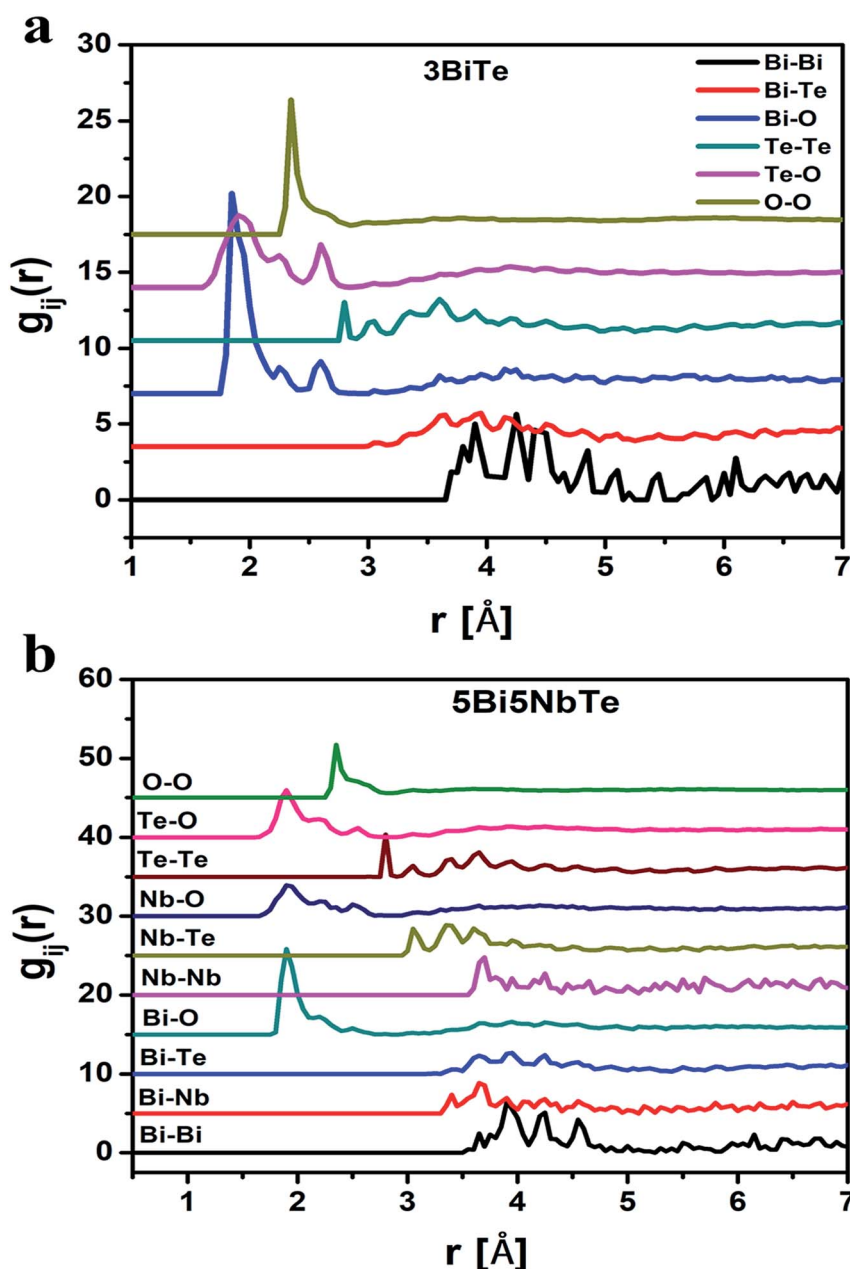

Fig. 5   Partial atomic pair correlation functions for the sample (a) 3BiTe ($3Bi_2O_3-97TeO_2$), and (b) 5Bi5NbTe ($5Bi_2O_3-5Nb_2O_5-90TeO_2$). The successive curves have been shifted by 3 and 5 units in (a) and (b) respectively for clarity.

monoclinic $Bi_2Te_4O_{11}$ anti-glass phase (Fig. 1a). On the other hand, despite the sharp X-ray diffraction peaks, the Raman spectra (Fig. 1b) shows broad bands for the bismuth tellurite sample containing 20 mol% Bi_2O_3. The striking difference in the Raman and X-ray diffraction patterns confirms the anti-glass nature of the bismuth tellurite sample containing 20 mol% Bi_2O_3 (Fig. 1a). The scattered X-ray intensity, I *vs.* Q data for bismuth tellurite and bismuth niobium tellurite glass and anti-glass samples is shown in Fig. 1a and 2.

The RMC calculated structure factors $S(Q)$, matched well with the experimental ones for all the glass samples and the fitted curves are shown in Fig. 3a and b for bismuth tellurite and

bismuth niobium tellurite glasses respectively. The reduced pair correlation functions, $G(r)$ were calculated by the Fourier transformation of $S(Q)$ data. $G(r)$ distributions for the bismuth tellurite and bismuth niobium tellurite samples are shown in Fig. 4a and b respectively. The intensity of the first peak at 1.90 Å decreases steadily with an increase in modifier oxide concentration (Bi_2O_3 and Nb_2O_5 mol%), this is because the first peak at 1.90 A is mainly due to Te–O equatorial bonds and the weight factors of these correlations decrease with an increase in Bi_2O_3 and Nb_2O_5 concentration in both the glass series. According to the earlier reports, the peaks due to Bi–O and Bi–Bi correlations lie at: 2–3 Å and ~4 Å respectively. Since $G(r)$ gives
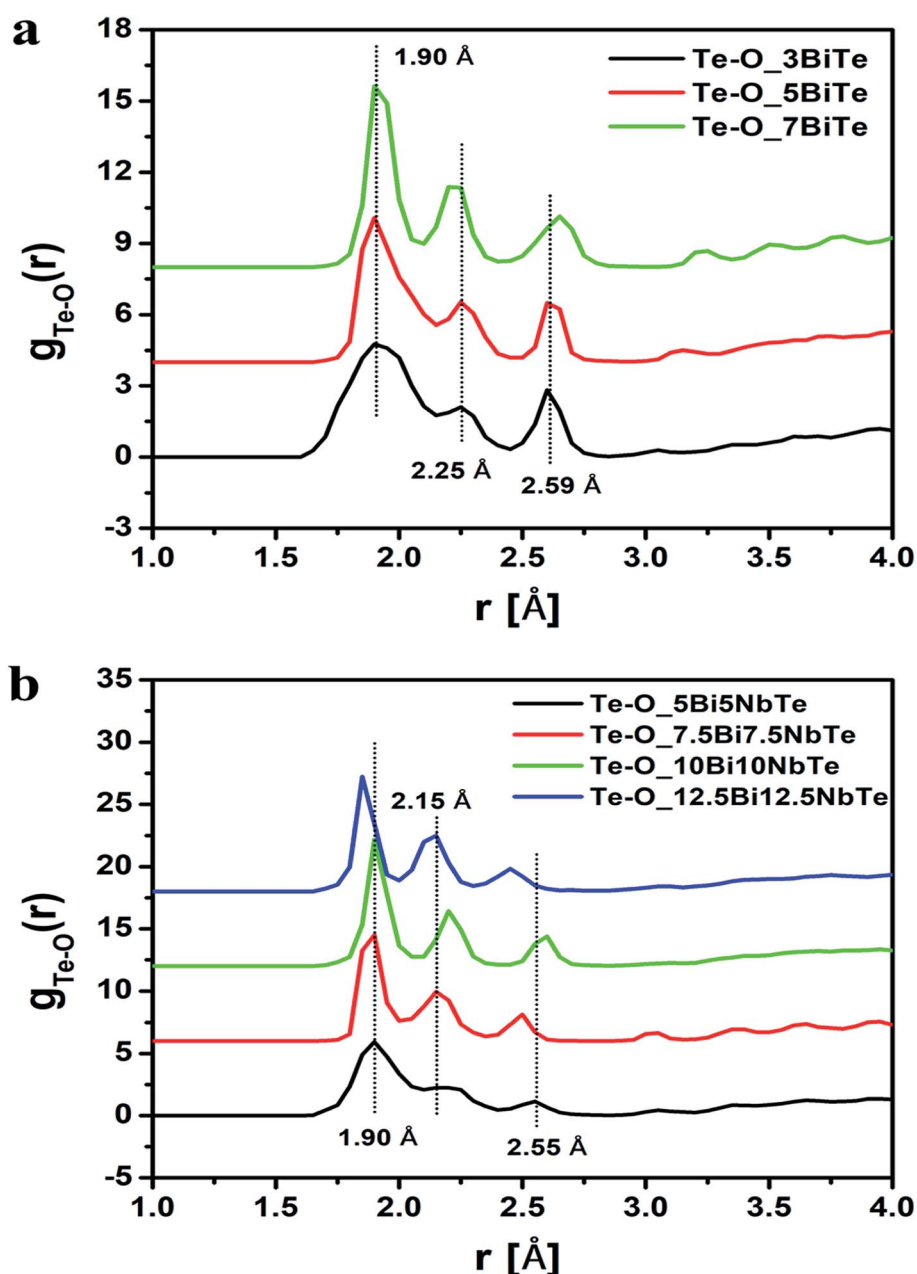

Fig. 6 (a) Te−O pair correlation functions in bismuth tellurite glasses and (b) in bismuth niobium tellurite glasses. The successive curves have been displaced by 3 units for clarity.

Table 7 Values of r_{min} and r_{max} used in the RMC for the calculation of Te–O coordination in bismuth tellurite glasses and bismuth niobium tellurite glasses

Sample code	Te–O		
	r_{min} (Å)	r_{max} (Å)	N_{Te-O}
3BiTe	1.60	2.45	4.17
5BiTe	1.65	2.46	3.89
7BiTe	1.66	2.40	3.67
5Bi5NbTe	1.60	2.40	3.85
7.5Bi7.5NbTe	1.67	2.35	3.81
10Bi10NbTe	1.65	2.39	3.76
12.5Bi12.5NbTe	1.65	2.30	3.56

the weighted sum of all the atomic pair correlations, it is difficult to de-convolute the multiple overlapping peaks and get accurate information about bond-lengths and co-ordination numbers, therefore, the partial atomic pair correlation functions were determined by the RMC technique.

The RMC method generates the partial atomic pair correlation functions, $g_{ij}(r)$ which provide structural information such as the nearest neighbor distances, bond angles and the co-ordination numbers. Fig. 5a and b give the partial pair distribution functions for various correlations in bismuth tellurite sample containing 3 mol% of Bi_2O_3 and bismuth niobium tellurite sample containing 5 mol% Nb_2O_5 and 5 mol% of Bi_2O_3. The partial atomic pair distribution functions for Te–O correlations ($g_{Te-O}(r)$) in bismuth tellurite glasses and bismuth niobium tellurite glasses are shown separately in Fig. 6a and b. It is found that Te–O linkages have a distribution of bond lengths and there exist at least three types of Te–O bonds of lengths of 1.90, 2.25 and 2.55 Å in glasses. The findings from the structural study of TeO_2 glass by Barney et al.[6] matches well with our results. Further the high-Q neutron and X-ray diffraction study by Hoppe et al.[43] on short-range order in ZnO–TeO_2 and Nb_2O_5–TeO_2 glasses reported the Te–O bond length to be 1.90 Å,

these earlier authors did not calculate the partial atomic pair correlation functions and were unable to resolve the axial and equatorial Te–O bonds in the glass network, which has been accomplished in the present study.

Theoretical predictions[44] of the short-range structural properties of tellurite glasses have revealed the existence of the wide distribution of Te–O bond lengths: two longer axial bonds in the range: 2.05 to 2.25 Å, and the two shorter equatorial Te–O bonds lengths at 1.85–1.95 Å. Therefore the second peak in the Te–O partial pair correlation function ($g_{Te-O}(r)$) is due to the longer Te–O axial bonds (Fig. 6a and b). The structural study of alkali tellurite glasses by X-ray diffraction brings forth the existence of highly asymmetrical Te–O pair distribution function.[6,8,45,46] Another peak in Te–O correlations has been observed in the range 2.5–2.6 Å, which reveals the presence of longer but more weakly bonded Te–O linkages, similar to the ones in crystalline γ-TeO_2.[47]

The structural interpretation of bismuth borate glasses had earlier suggested that most of the bismuth-containing compositions contain two types of Bi–O bonds at ∼1.9 Å and 2.5 Å.[48] However, Stone et al.[49] reported the existence of Bi–O bonds at 1.95 Å and 2.37 Å. The pair correlation function for Bi–O shows the existence of three peaks centered at 1.90 Å, 2.20 Å, and 2.59 Å. According to Dimitriev et al.,[50] the first maxima for Bi–O correlation in the bismuthate glasses appears around ∼2.2–2.4 Å. Watanabe et al.[51] also reported the Bi–O bond length to be in the range: 2 to 3 Å. The findings of the present study are therefore in agreement with the earlier studies.

The r_{min} and r_{max} values from the $g_{Te-O}(r)$ plots were used to calculate the co-ordination number of tellurium with oxygens (N_{Te-O}) in glass samples. The r_{min} and r_{max} values for Te–O bonds and the calculated coordination number are given in Table 7. The average value of N_{Te-O} in bismuth tellurite glass series decreases from 4.17 to 3.67 upon increasing the Bi_2O_3 concentration from 3 to 7 mol%. In bismuth niobium tellurite glasses, the N_{Te-O} decreases from 3.85 to 3.56 upon increasing the Bi_2O_3 and Nb_2O_5 content from 5 to 12.5 mol%. It may be
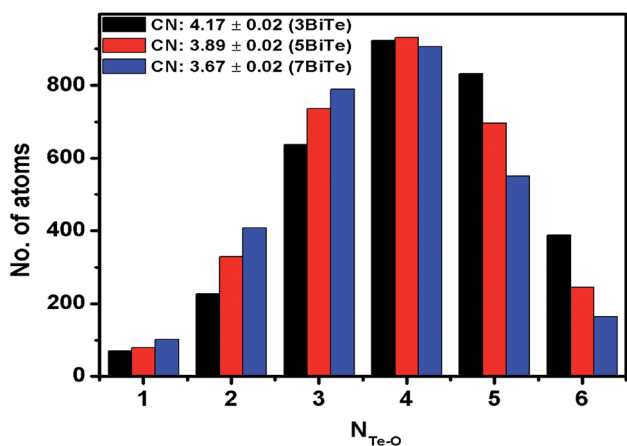
Fig. 7 N_{Te-O} for bismuth tellurite glasses calculated using RMC simulations.
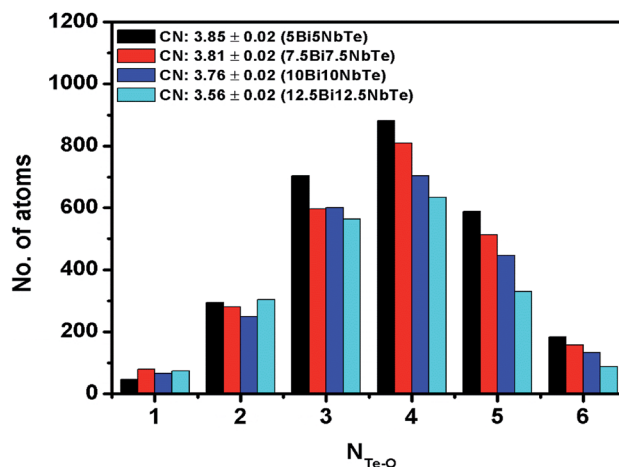
Fig. 8 N_{Te-O} for bismuth niobium tellurite glasses calculated using RMC simulations.

noted that the area under the third peak is not taken into account while calculating the N_{Te-O} values, therefore the r_{max} is taken only up to the point where the second Te–O peak tails off, since it is reported that r_{max} for the first Te–O co-ordination shell ends at 2.36 Å.[45,52]

Raman studies on various tellurite glasses show that, the N_{Te-O} decreases with an increase in the concentration of modifier oxides due to the transformation of trigonal bipyramidal units (TeO$_4$) into trigonal pyramidal (TeO$_3$) units.[6,14,53–56] The structural interpretation of alkali-tellurite glasses by neutron diffraction, X-ray diffraction, and RMC simulations found the transformation of TeO$_4$ into TeO$_3$ units takes place via the formation of TeO$_{3+1}$ polyhedra as the intermediate structural unit: TeO$_4$ → TeO$_{3+1}$ → TeO$_4$.[57] The distribution of Te–O co-ordinations in bismuth tellurite glasses and bismuth

niobium tellurite glasses as found by RMC simulations is presented in Fig. 7 and 8 respectively. The bar graphs represent the variation of the average coordination number for tellurium with oxygens and reveal an increase in trigonal tellurite units accompanied by a decrease in tetrahedral tellurite units. The bar graphs also suggests the presence of small amounts of penta and hexa-tellurite units which decrease with increase in the modifier oxide concentration in both, bismuth tellurite and bismuth niobium tellurite glasses. An estimate of Bi–O speciation shows a decrease in the Bi–O coordination number from 5.64 to 4.62 with increase in Bi$_2$O$_3$ content.

The bond angles O–Te–O, O–O–O and Te–O–Te were calculated from the RMC results using the r_{max} value of partial pair correlation functions. The bond angle distribution for Te–O–Te, O–Te–O and O–O–O linkages for bismuth tellurite glasses are
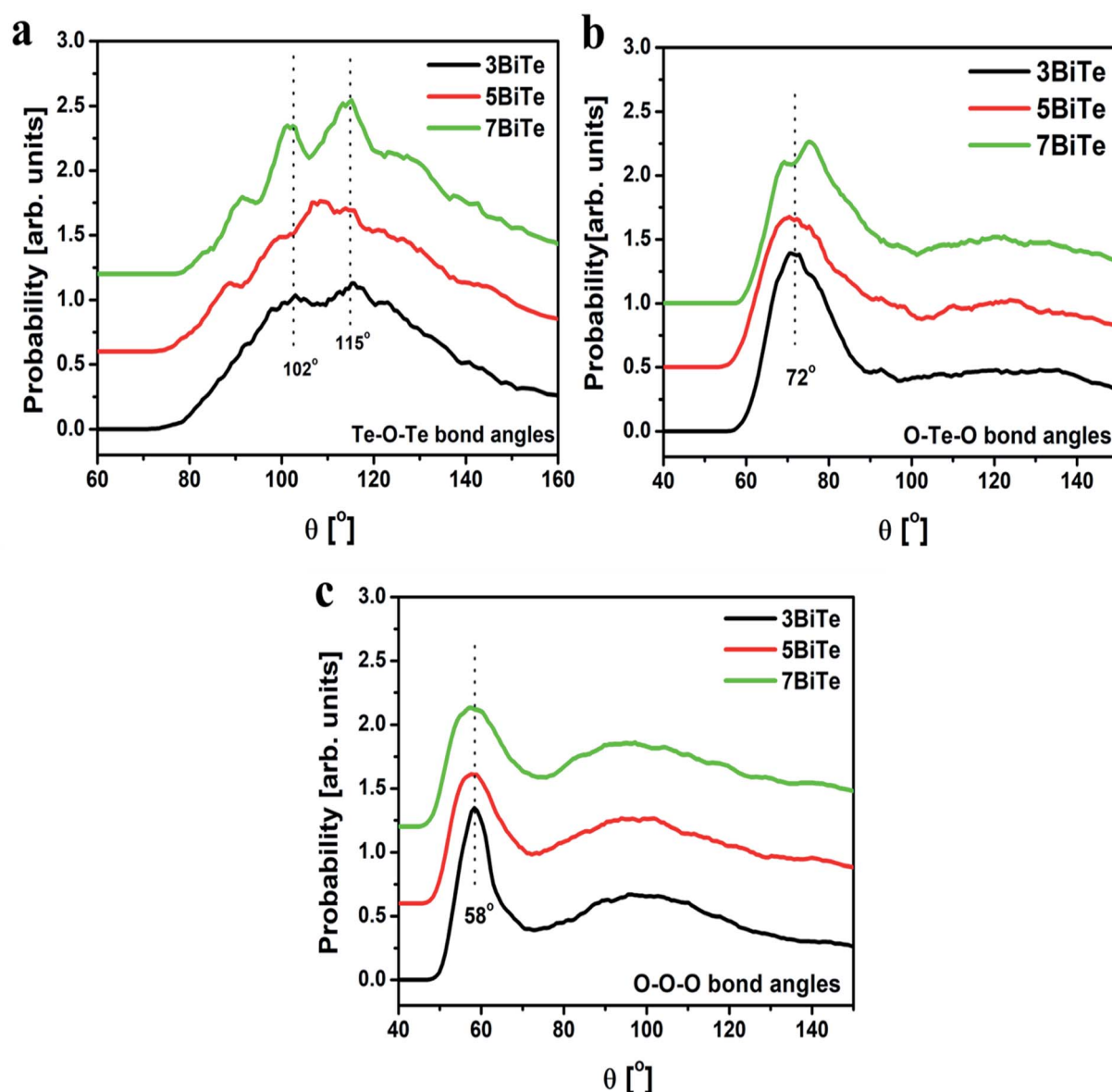

Fig. 9 Bond angle distributions for (a) Te−O−Te, (b) O−Te−O and (c) O−O−O linkages in three bismuth tellurite glasses. Successive curves have been shifted by 0.6 units for clarity.

presented in Fig. 9(a–c), while the plots for bond angle distributions in bismuth niobium tellurite glasses are shown in Fig. 10(a–c). The bond angle distribution for O–Te–O linkages in tellurite glasses generally show two peaks, one in the range 150–170° due to O_{ax}–Te–O_{ax} axial linkages, while the other one in the range: 70–105° is due to the O_{eq}–Te–O_{eq} and O_{eq}–Te–O_{ax} linkages.[44] In bismuth tellurite and bismuth niobium tellurite glasses, the O–Te–O maxima occurs at the lower angle of ~72–74° which reveals that the major part of the glass network consists of O_{eq}–Te–O_{eq} and O_{eq}–Te–O_{ax} bonds in TeO_3 and TeO_4 structural units containing bridging, non-bridging and terminal oxygens. The absence of the peaks in the higher angle ranges confirms the presence of a very small concentration of axial (O_{ax}–Te–O_{ax}) linkages.

Te–O–Te bond angle distribution represents the connectivity between the TeO_3 and TeO_4 units and the intermediate range order in glass. The Te–O–Te bond angles in the bismuth tellurite glasses consists of peaks at 102° and 115° while a new peak at 88° emerges with an increase in the modifier oxide concentration. On the other hand, a wider distribution of Te–O–Te bond angles is observed in bismuth niobium tellurite glasses in the range: 86–130°.

3.3. Rietveld refinement results on anti-glass $Bi_2Te_4O_{11}$

The HEXRD pattern for bismuth tellurite sample containing 20 mol% Bi_2O_3 (sample 20BiTe) show sharp peaks characteristic of crystalline material, however its vibrational spectra (Raman
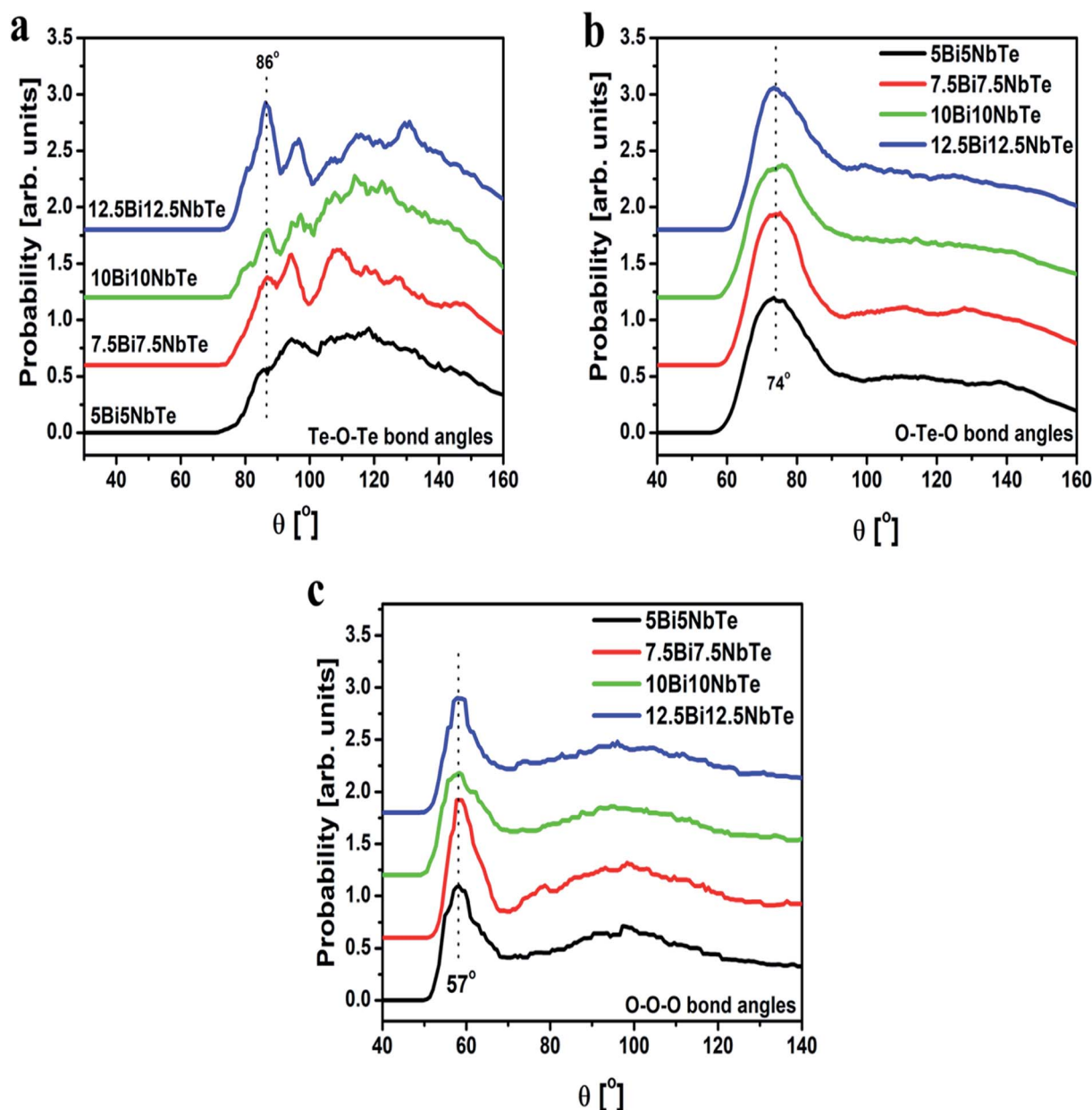

Fig. 10 Bond angle distributions for (a) Te−O−Te, (b) O−Te−O and (c) O−O−O linkages in four bismuth niobium tellurite glasses. Successive curves have been shifted by 0.6 units for clarity.
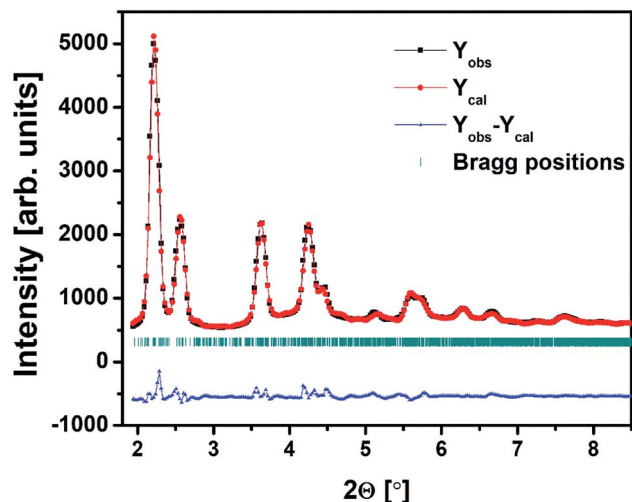
Fig. 11 Rietveld fit of the high-energy XRD data for bismuth tellurite sample containing 20 mol% Bi_2O_3.

Table 8 Fractional co-ordinates of Bi, Te, and O in the unit cell of anti-glass $Bi_2Te_4O_{11}$

Atom	x	y	z
Bi1	0.587 ± 0.023	0.120 ± 0.003	0.420 ± 0.012
Bi2	0.570 ± 0.006	0.111 ± 0.002	0.913 ± 0.006
Te1	0.277 ± 0.010	0.160 ± 0.018	0.241 ± 0.005
Te2	0.914 ± 0.009	0.119 ± 0.006	0.574 ± 0.005
Te3	0.242 ± 0.008	0.090 ± 0.002	0.755 ± 0.004
Te4	0.893 ± 0.008	0.139 ± 0.011	0.071 ± 0.002
O1	0.941 ± 0.004	0.170 ± 0.021	0.478 ± 0.010
O2	0.921 ± 0.139	0.172 ± 0.002	0.971 ± 0.029
O3	0.270 ± 0.044	0.159 ± 0.013	0.585 ± 0.013
O4	0.275 ± 0.033	0.145 ± 0.031	0.345 ± 0.054
O5	0.562 ± 0.051	0.025 ± 0.051	0.764 ± 0.002
O6	0.954 ± 0.040	0.153 ± 0.011	0.751 ± 0.004
O7	0.644 ± 0.049	0.071 ± 0.005	0.541 ± 0.015
O8	0.348 ± 0.085	0.169 ± 0.031	0.107 ± 0.026
O9	0.671 ± 0.023	0.020 ± 0.230	0.036 ± 0.005
O10	0.802 ± 0.077	0.104 ± 0.005	0.190 ± 0.054
O11	0.310 ± 0.014	0.223 ± 0.065	0.835 ± 0.023

patterns) reveal the presence of broad phonon bands that are the characteristic feature of disordered/amorphous materials. Trömel et al.[17] referred these materials as the 'anti-glass' where order and disorder co-exists. Masson et al.[41] suggest these materials as an intermediate state between a glass and crystalline phase containing disturbed short-range order while the arrangement of cations is ordered and indicate the process of crystallization. It is reported that the structure of disordered anti-glass $Bi_2Te_4O_{11}$ is comprised of a sequence of two layers of cations. Layer one contains only the tellurite units with TeO_3 and TeO_4 units forming long sinusoidal chains, similar to the ones present in paratellurite α-TeO_2.[58] The second layer is a composite layer containing both the bismuth and the tellurium atoms in equal number.

The XRD pattern recorded for 20BiTe is shown in Fig. 1a. All the peaks can be indexed to $P12_1/n1$ space group of monoclinic symmetry. The diffraction pattern exhibits significant extra broadening on top of the instrumental resolution which indicates that the long-range order in this sample is also not well defined. This suggests that the sample is not crystalline but an 'anti-glass' of monoclinic $Bi_2Te_4O_{11}$ (powder diffraction file #81-1330).[18]

The HEXRD data of 20Bi_2O_3–80TeO_2 anti-glass sample was refined by Rietveld method using FULLPROF program. The refined XRD pattern of 20BiTe sample is shown in Fig. 11 and the position co-ordinates of constituents atoms namely Bi, Te, and O are given in Table 8. The values of cell parameters obtained after refinement were $a = 6.89$ Å, $b = 7.97$ Å, and $c = 19.65$ Å, and $\alpha = \gamma = 90°$ with $\beta = 91.26°$.

The other structural parameters such as bond lengths, cation coordination number, and bond angles for 20BiTe anti-glass sample were calculated from the VESTA program.[42] Fig. 12 shows $Bi_2Te_4O_{11}$ unit cell obtained from the refinement of HEXRD data. As discussed by Masson et al.[41] the unit cell clearly shows the structure comprised of two cation-oxygen layers, where one layer contains only tellurite units while the other

contains both Te and Bi ions. Since the unit cell structure comprises two layers of Te–O units, the mean value of Te–O coordination, N_{Te-O} in this sample was calculated from both the layers with VESTA program. The average N_{Te-O} value in $Bi_2Te_4O_{11}$ anti-glass sample is 2.96 and its value is significantly lower than the value of N_{Te-O} in bismuth tellurite glasses, this result is also confirmed from Raman studies (Fig. 1b) in which the intensity of the Raman band at ∼660 cm^{-1} is significantly suppressed as compared to the intensity of Raman band at ∼770 cm^{-1} and is due to the structural transformation: $TeO_4 \rightarrow TeO_3$ that takes place with increase in Bi_2O_3 concentration from 3 to 20 mol%. Since the sample 20BiTe has highest Bi_2O_3
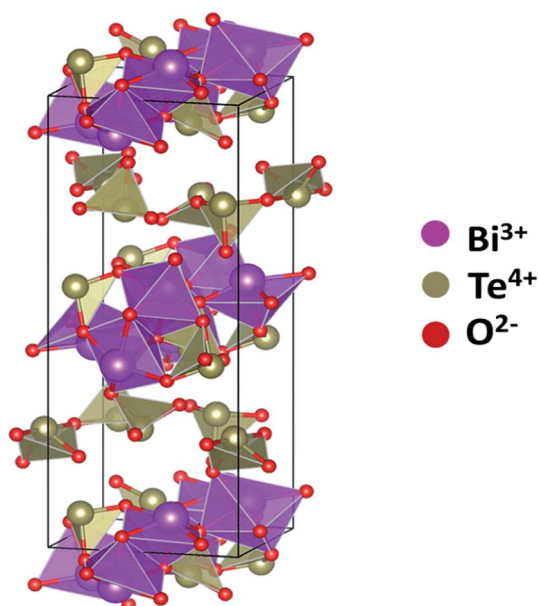

Fig. 12 Unit cell of monoclinic anti-glass $Bi_2Te_4O_{11}$ showing Bi (purple), tellurium (grey) and oxygen (red) ions.

concentration (20 mol%), it has the smallest N_{Te-O}. A lower value of N_{Te-O} in this sample also indicates the presence of oxygen vacancies; the latter is a characteristic feature of anti-glass materials. The Te–O bond length in the anti-glass 20BiTe sample is in the range: 1.939–2.046 Å, nBi–O bond lengths are in the range; 2.372–2.392 Å and the mean Bi–O coordination, N_{Bi-O} is 4.17.

The angle distribution of O–Te–O bonds in the anti-glass sample depends upon the internal angles of inter and intra polyhedral TeO_3 and TeO_4 structural units. Among TeO_3 units the angles lies in the range ∼90° to 103° while in the case of TeO_4 units, the angle O_{ax}–Te–O_{ax} was estimated to be ∼178°, the latter O–Te–O bond angle linkages were absent in the bismuth tellurite glasses, while the O_{eq}–Te–O_{ax} bond angle was found to be 92°. The Te–O–Te bond angle was found to be ∼144°, equivalent to the one found in α-TeO_2.[59] The bond lengths were found to be Te–O_{eq} as 1.85 Å while the Te–O_{ax} is 2.03 Å. Moreover, no bond length greater than 2.4 Å was observed in this anti-glass sample unlike the bismuth tellurite glasses.

4. Conclusion

High-energy X-ray diffraction (HEXRD) studies on series of bismuth tellurite and bismuth niobium tellurite glasses and one anti-glass sample were carried out. Bismuth tellurite system forms glass only at a low concentration of Bi_2O_3 (up to 7 mol%), while at higher Bi_2O_3 (20 mol%) it forms purely anti-glass phase of the monoclinic $Bi_2Te_4O_{11}$ by more rapid splat-quenching. Owing to the latter's anti-glass nature, the diffraction pattern show sharp Bragg peaks whereas glasses show broad humps that are typical of an amorphous material. The RMC analysis of HEXRD data confirms that the nearest neighbor distance of Te–O and Bi–O are in the range of 1.85–1.90 Å and Te–O bonds have a distribution of bond lengths.

Te–O coordination number, N_{Te-O} decreases from 4.17 ± 0.02 to 3.67 ± 0.02 on increasing Bi_2O_3 concentration from 3 to 7 mol% in xBi$_2$O$_3$–(100 − x)TeO$_2$ system which further decreases to 3.56 ± 0.02 upon incorporating Nb_2O_5 in the bismuth tellurite system. The sample of composition, 20Bi$_2$O$_3$–80TeO$_2$ forms an anti-glass phase of disordered monoclinic $Bi_2Te_4O_{11}$ and shows sharp reflections in HEXRD. Structural refinement was carried out by FullProf Rietveld analysis and the unit cell parameters were determined. The mean value of Te–O coordination in 20BiTe anti-glass sample was calculated to be 2.96 ± 0.02 and is lower than that of glasses of xBi$_2$O$_3$–(100 − x) TeO$_2$ system.

Conflicts of interest

There are no conflicts to declare.

Acknowledgements

References

1 S. Suehara, P. Thomas, A. Mirgorodsky, T. Merle-Méjean, J. Champarnaud-Mesjard, T. Aizawa, S. Hishita, S. Todoroki, T. Konishi and S. Inoue, Localized hyperpolarizability approach to the origin of nonlinear optical properties in TeO$_2$-based materials, *Phys. Rev. B: Condens. Matter Mater. Phys.*, 2004, **70**, 205121.

2 V. Rivera and D. Manzani, *Technological Advances in Tellurite Glasses*, Springer, 2017.

3 D. Zhou, R. Wang, Z. Yang, Z. Song, Z. Yin and J. Qiu, Spectroscopic properties of Tm^{3+}-doped TeO$_2$-R$_2$O-La$_2$O$_3$ glasses for 1.47 μm optical amplifiers, *J. Non-Cryst. Solids*, 2011, **357**, 2409–2412.

4 S. Manning, in *A study of tellurite glasses for electro-optic optical fibre devices*, University of Adelaide, Adelaide, Australia, 2011.

5 I. Bányász, S. Berneschi, M. Bettinelli, M. Brenci, M. Fried, N. Khanh, T. Lohner, G. N. Conti, S. Pelli and P. Petrik, MeV Energy N$^+$-Implanted Planar Optical Waveguides in Er-Doped Tungsten-Tellurite Glass Operating at 1.55 mm, *IEEE Photonics J.*, 2012, **4**, 721–727.

6 E. R. Barney, A. C. Hannon, D. Holland, N. Umesaki, M. Tatsumisago, R. G. Orman and S. Feller, Terminal oxygens in amorphous TeO$_2$, *J. Phys. Chem. Lett.*, 2013, **4**, 2312–2316.

7 N. Tagiara, D. Palles, E. Simandiras, V. Psycharis, A. Kyritsis and E. Kamitsos, Synthesis, thermal and structural properties of pure TeO$_2$ glass and zinc-tellurite glasses, *J. Non-Cryst. Solids*, 2017, **457**, 116–125.

8 A. Gulenko, O. Masson, A. Berghout, D. Hamani and P. Thomas, Atomistic simulations of TeO$_2$-based glasses: interatomic potentials and molecular dynamics, *Phys. Chem. Chem. Phys.*, 2014, **16**, 14150–14160.

9 R. A. El-Mallawany, *Tellurite glasses handbook: Physical Properties and Data*, CRC press, Boca Raton, 2016.

10 T. Hasegawa, T. Nagashima and N. Sugimoto, Determination of nonlinear coefficient and group-velocity-dispersion of bismuth-based high nonlinear optical fiber by four-wave-mixing, *Opt. Commun.*, 2008, **281**, 782–787.

11 H. Ebendorff-Heidepriem, P. Petropoulos, V. Finazzi, K. Frampton, R. Moore, D. Richardson and T. Monro, Highly nonlinear bismuth-oxide-based glass holey fiber, in *Optical Fiber Communication Conference*, Optical Society of America, 2004, pp. ThA4.

12 K. Kikuchi and K. Taira, Highly nonlinear bismuth oxide-based glass fibres for all-optical signal processing, *Electron. Lett.*, 2002, **38**, 166–167.

13 J. He, H. Zhan and A. Lin, Solid-core bismuth–tellurite glass fiber with low propagation loss and high nonlinearity, *Mater. Res. Bull.*, 2019, 110619.

14 A. Kaur, A. Khanna, H. Bhatt, M. Gónzález-Barriuso, F. González, B. Chen and M. Deo, B-O and Te-O speciation in bismuth tellurite and bismuth borotellurite glasses by FTIR, ¹¹B MAS-NMR and Raman spectroscopy, *J. Non-Cryst. Solids*, 2017, **470**, 19–26.

15 M. Trömel, E. Münch, G. Blasse and G. Dirksen, Formation and luminescence of lower symmetrical tellurite anti-glass phases, *J. Solid State Chem.*, 1988, **76**, 345–354.

16 A. Bertrand, J. Carreaud, G. l. Delaizir, M. Shimoda, J.-R. Duclére, M. Colas, M. Belleil, J. Cornette, T. Hayakawa and C. c. Genevois, New Transparent Glass-Ceramics Based on the Crystallization of "Anti-glass" Spherulites in the Bi₂O₃–Nb₂O₅–TeO₂ System, *Cryst. Growth Des.*, 2015, **15**, 5086–5096.

17 M. Trömel, W. Hützler and E. Münch, Anti-glass phases and other lanthanide tellurates with fluorite-related structures, *J. Less Common Met.*, 1985, **110**, 421–424.

18 N. Gupta and A. Khanna, Glass and anti-glass phase co-existence and structural transitions in bismuth tellurite and bismuth niobium tellurite systems, *J. Non-Cryst. Solids*, 2018, **481**, 594–603.

19 R. Kaur, A. Khanna, M. González-Barriuso, F. González and B. Chen, Structural, optical and thermal properties of glass and anti-glass phases in strontium tellurite and borotellurite systems doped with europium, *Mater. Res. Bull.*, 2018, **106**, 288–295.

20 S. Baki, L. Tan, C. Kan, M. K. Halimah and M. Mahdi, Structural and Optical Characteristics of Erbium Doped Ternary TeO₂-TiO₂-Bi₂O₃ Glasses, in *Solid State Phenomena*, Trans Tech Publ, 2017, pp. 148–154.

21 A. Kaur, A. Khanna and M. Fábián, Short-range structure of barium tellurite glasses and its correlation with stress-optic response, *Mater. Res. Express*, 2018, **5**, 065203.

22 J. D. Musgraves, J. Hu and L. Calvez, *Springer Handbook of Glass*, Springer, 2019.

23 R. Limbach, A. Winterstein-Beckmann, J. Dellith, D. Möncke and L. Wondraczek, Plasticity, crack initiation and defect resistance in alkali-borosilicate glasses: from normal to anomalous behavior, *J. Non-Cryst. Solids*, 2015, **417**, 15–27.

24 S. Inaba and S. Fujino, Empirical equation for calculating the density of oxide glasses, *J. Am. Ceram. Soc.*, 2010, **93**, 217–220.

25 M. C. Wilding, G. Delaizir, C. J. Benmore, Y. Gueguen, M. Dolhen, J.-R. Duclère, S. Chenu, S. Sukenaga and P. F. McMillan, Structural studies of Bi₂O₃-Nb₂O₅-TeO₂ glasses, *J. Non-Cryst. Solids*, 2016, **451**, 68–76.

26 M. Fábián and C. Araczki, Basic network structure of SiO₂–B₂O₃–Na₂O glasses from diffraction and reverse Monte Carlo simulation, *Phys. Scr.*, 2016, **91**, 054004.

27 H. Poulsen, J. Neuefeind, H.-B. Neumann, J. Schneider and M. Zeidler, Amorphous silica studied by high energy X-ray diffraction, *J. Non-Cryst. Solids*, 1995, **188**, 63–74.

28 N. Sahu and S. Panigrahi, Mathematical aspects of Rietveld refinement and crystal structure studies on PbTiO₃ ceramics, *Bull. Mater. Sci.*, 2011, **34**, 1495–1500.

29 N. Gupta, A. Kaur, A. Khanna, F. Gonzàlez, C. Pesquera, R. Iordanova and B. Chen, Structure-property correlations

in TiO₂-Bi₂O₃-B₂O₃-TeO₂ glasses, *J. Non-Cryst. Solids*, 2017, **470**, 168–177.

30 N. Schell, A. King, F. Beckmann, T. Fischer, M. Müller and A. Schreyer, The high energy materials science beamline (HEMS) at PETRA III, in *Materials Science Forum*, Trans Tech Publ, 2014, pp. 57–61.

31 X. Qiu, J. W. Thompson and S. J. L. Billinge, PDFgetX2: a GUI-driven program to obtain the pair distribution function from X-ray powder diffraction data, *J. Appl. Crystallogr.*, 2004, **37**, 678.

32 H. E. Fischer, A. C. Barnes and P. S. Salmon, Neutron and x-ray diffraction studies of liquids and glasses, *Rep. Prog. Phys.*, 2005, **69**, 233.

33 L. B. Skinner, C. J. Benmore and J. B. Parise, Area detector corrections for high quality synchrotron X-ray structure factor measurements, *Nucl. Instrum. Methods Phys. Res., Sect. A*, 2012, **662**, 61–70.

34 J. H. Hubbell and L. Overbro, Relativistic atomic form factors and photon coherent scattering cross sections, *J. Phys. Chem. Ref. Data*, 1979, **8**, 69–106.

35 B. Toby and T. Egami, Accuracy of pair distribution function analysis applied to crystalline and non-crystalline materials, *Acta Crystallogr., Sect. A: Found. Crystallogr.*, 1992, **48**, 336–346.

36 R. L. McGreevy and L. Pusztai, Reverse Monte Carlo Simulation: A New Technique for the Determination of Disordered Structures, *Mol. Simul.*, 1988, **1**, 359–367.

37 G. Evrard and L. Pusztai, Reverse Monte Carlo modelling of the structure of disordered materials with RMC++: a new implementation of the algorithm in C++, *J. Phys.: Condens. Matter*, 2005, **17**, S1.

38 M. Fabian, E. Svab and K. Krezhov, Network structure with mixed bond-angle linkages in MoO₃–ZnO–B₂O₃ glasses: neutron diffraction and reverse Monte Carlo modelling, *J. Non-Cryst. Solids*, 2016, **433**, 6–13.

39 O. Gereben, P. Jóvári, L. Temleitner and L. Pusztai, A new version of the RMC++ Reverse Monte Carlo programme, aimed at investigating the structure of covalent glasses, *J. Optoelectron. Adv. Mater.*, 2007, **9**, 3021–3027.

40 P. A. Egelstaff, 14 Classical Fluids, in *Methods in Experimental Physics*, Elsevier, 1987, pp. 405–470.

41 O. Masson, P. Thomas, O. Durand, T. Hansen, J. Champarnaud and D. Mercurio, On the structure of the disordered Bi₂Te₄O₁₁ phase, *J. Solid State Chem.*, 2004, **177**, 2168–2176.

42 K. Momma and F. Izumi, VESTA 3 for three-dimensional visualization of crystal, volumetric and morphology data, *J. Appl. Crystallogr.*, 2011, **44**, 1272–1276.

43 U. Hoppe, E. Yousef, C. Rüssel, J. Neuefeind and A. Hannon, Structure of zinc and niobium tellurite glasses by neutron and x-ray diffraction, *J. Phys.: Condens. Matter*, 2004, **16**, 1645.

44 F. Pietrucci, S. Caravati and M. Bernasconi, TeO₂ glass properties from first principles, *Phys. Rev. B: Condens. Matter Mater. Phys.*, 2008, **78**, 064203.

45 V. Kozhukharov, S. Neov, I. Gerasimova and P. Mikula, Neutron diffraction investigation of a tellurite-tungstate glass, *J. Mater. Sci.*, 1986, **21**, 1707–1714.

46 J. McLaughlin, S. Tagg, J. Zwanziger, D. Haeffner and S. Shastri, The structure of tellurite glass: a combined NMR, neutron diffraction, and X-ray diffraction study, *J. Non-Cryst. Solids*, 2000, **274**, 1–8.

47 J. Champarnaud-Mesjard, S. Blanchandin, P. Thomas, A. Mirgorodsky, T. Merle-Mejean and B. Frit, Crystal structure, Raman spectrum and lattice dynamics of a new metastable form of tellurium dioxide: γ-TeO_2, *J. Phys. Chem. Solid.*, 2000, **61**, 1499–1507.

48 A. C. Wright, S. A. Feller and A. C. Hannon, *Borate glasses, crystals & melts*, Society of Glass Technology, 1997.

49 C. Stone, A. Wright, R. Sinclair, S. Feller, M. Affatigato, D. Hogan, N. Nelson, C. Vira, Y. Dimitriev and E. Gattef, Structure of bismuth borate glasses, *Phys. Chem. Glasses*, 2000, **41**, 409–412.

50 Y. Dimitriev, A. Wright, V. Mihailova, E. Gattef and C. Guy, An X-ray diffraction study of bismuthate glasses, *J. Mater. Sci. Lett.*, 1995, **14**, 347–350.

51 T. Watanabe, T. Nanba and Y. Miura, X-ray and neutron scattering study of the structure of lithium bismuth oxide glass, *J. Non-Cryst. Solids*, 2002, **297**, 73–83.

52 A. Khanna, M. Fábián, P. Krishna, C. J. Benmore, A. Kaur, A. Kaur, A. Shinde, P. Rajput and S. Jha, Structural analysis of WO_3-TeO_2 glasses by neutron, high energy X-ray diffraction, reverse Monte Carlo simulations and XANES, *J. Non-Cryst. Solids*, 2018, **495**, 27–34.

53 A. G. Kalampounias, Low-frequency Raman scattering in alkali tellurite glasses, *Bull. Mater. Sci.*, 2008, **31**, 781–785.

54 A. Kaur, A. Khanna, V. G. Sathe, F. Gonzalez and B. Ortiz, Optical, thermal, and structural properties of Nb_2O_5–TeO_2 and WO_3–TeO_2 glasses, *Phase Transitions*, 2013, **86**, 598–619.

55 T. Sekiya, N. Mochida and A. Ohtsuka, Raman spectra of MO-TeO_2 (M= Mg, Sr, Ba and Zn) glasses, *J. Non-Cryst. Solids*, 1994, **168**, 106–114.

56 M. R. Zaki, D. Hamani, M. Dutreilh-Colas, J.-R. Duclère, O. Masson and P. Thomas, Synthesis, thermal, structural and linear optical properties of new glasses within the TeO_2-TiO_2-WO_3 system, *J. Non-Cryst. Solids*, 2018, **484**, 139–148.

57 H. Munemura, K. Mitome, M. Misawa and K. Maruyama, Network structure of M_2O–TeO_2 (M= Li, Na, Li0. 62Na0.38) glasses, *J. Non-Cryst. Solids*, 2001, **293**, 700–704.

58 P. Thomas, The crystal structure and absolute optical chirality of paratellurite, α-TeO_2, *J. Phys. C: Solid State Phys.*, 1988, **21**, 4611.

59 E. Barney, A. Hannon and D. Holland, Short-range order and dynamics in crystalline α-TeO_2, *J. Phys. Chem. C*, 2012, **116**, 3707–3718.